International Journal of Steel Structures (2022) 22(2):566–584
https://doi.org/10.1007/s13296-022-00591-5

Online ISSN 2093-6311
Print ISSN 1598-2351

Seismic Performance of Welded Steel Beam-to-Column Connections with Initial Weld Defects

Jiaming Li[1,2] · Haoran Yu[1,2] · Weibin Li[1,2] · Weijia Cheng[1,2]

Received: 29 July 2021 / Accepted: 18 February 2022 / Published online: 25 March 2022

Abstract
Based on the research of steel structures destroyed in earthquakes, it is often found that brittle fractures of the bottom beam flanges of welded beam-to-column connections are caused by welding defects. In this study, artificial surface notches in the welds of single beam flanges were prepared, and four experimental specimens of welded steel beam-to-column connections were tested to explore the effects of the initial crack and three different connection types on the seismic performance of the connections. Through extended finite element methods, the factor of the depth of the initial crack was discussed. The results showed that the fracture mode and the rate and location of crack propagation are significantly changed, and the seismic performance of the connections is reduced when there is an initial crack existing in the weld of a single beam flange. The fracture in box beam to box column connections shows brittle failure regardless of the initial crack, but the depth of the initial crack has the least influence on their seismic performance among the three connection types. The seismic performance of H-shaped beam to H-shaped column connections is the most sensitive to the depth of the initial crack. It should be noted that the weld quality of steel beam-to-column connections, especially the connections with H-shaped columns, should be carefully checked and monitored during the welding construction process and after earthquakes to ensure the bearing and deformation capacities meeting the requirements.

Keywords Welded steel beam-to-column connections · Seismic performance · Initial crack · Crack propagation · Failure mode · Extended finite element method

1 Introduction

Beam-to-column connections are an essential part of steel moment-resisting frames, and the strength and stiffness of the connections have a significant influence on the overall structural performance. In the 1994 Northridge earthquake and the 1995 Hyogo-ken Nanbu earthquake, many steel structures were severely destroyed and showed brittle failure even though the design fully met the requirements of specifications (Tremblay et al., 1996; Miller, 1998; Popov, 1998).

In these destroyed steel structures, the weld at the bottom beam flange of beam-to-column connections was one of the most seriously damaged areas (AISC, 1994; Kauffmann & Fisher, 1996; SAC Joint Venture, 1995a; Song & Ellingwood, 1999). Some of the explanations for this phenomenon are stress concentrations caused by a combination of factors such as welding defects and inevitable structural forms (Chi et al., 2000). In practical engineering, the dispersion of welding quality is quite large even if it meets the quality requirements (Engelhardt & Sabol, 1997). Many defects are easy to ignore and hard to detect, such as local cracks caused by welding interruption during overhead operation, and unoccluded penetration cracks due to the obstruction of welding brackets or little slag and bubbles in the weld. Moreover, cracks may appear in these welds after earthquakes but the connection has not been timely reinforced and repaired, then it gets greater damage in aftershocks. All these factors may become the beginning of crack initiation and propagation.

✉ Weibin Li
liwbseu@vip.163.com

Jiaming Li
scorpion.jere@qq.com

[1] Key Laboratory of Concrete and Prestressed Concrete Structures of Ministry of Education, Southeast University, Nanjing 211189, China

[2] School of Civil Engineering, Southeast University, Nanjing 211189, China

When crack initiation or propagation occurs in the weld of steel beam-to-column connections under an earthquake action, the seismic performance of the connections is reduced and brittle fractures may eventually occur, which brings adverse effects to the overall structural performance and post-earthquake repair. To investigate the failure behaviors of steel beam-to-column connections, SAC Joint Venture had conducted several experimental full-scale tests under dynamic and static loads (Anderson et al., 1995; Jones et al., 2002; SAC Joint Venture, 1995a, 1996), and verified the test results through finite element analysis. On this basis, stress and strain in the key parts of the connections were extracted to calculate the fracture mechanics indexes (Chi et al., 2000). Moreover, they also carried out a theoretical study on the impact of connection fractures on the overall structural behaviors, and proposed a method to predict the damage degree and fracture location (Anderson et al., 1995; SAC Joint venture, 1995b; SAC Joint venture, 1995; Gross, 1998). An et al. (2018) researched the effects of geometrical heterogeneity, strength mismatches, and loading rates on critical conditions of ductile fracture through ductile crack initiation tests under static and dynamic loading, and the results indicated that the condition for ductile crack initiation using the two-parameter criterion (involving equivalent plastic strain and stress triaxiality) is a transferable criterion to evaluate ductile crack initiation, which is independent of the existence of strength mismatches and loading rates. Liu et al. (2017) conducted nine full-scale tests on beam-to-column connections to analyze the effect of loading modes on connection, and developed an effective plastic strain index to evaluate the connection damage. Joh and Chen (1999) investigated the fracture strength of welded unreinforced flange-bolted web (WUF-B) connections using the method of linear elastic fracture mechanics, and proposed a new way to calculate the brittle fracture strength of connections according to the maximum energy release rate of crack tips at the failure moment. Matos and Dodds (2000, 2001, 2002) provided an eigenstrain approach to impose realistic residual stress fields on the weld of bottom beam flanges in three-dimensional (3D) finite element models, and proposed a theoretical model which can predict the cumulative failure probability as a function in the form of beam end moment. From the perspective of micro, Huang et al. (2013) proposed a numerical method based on micromechanics damage model instead of traditional fracture analytical methods to investigate the crack initiation and propagation of welded beam-to-column connections subjected to monotonic loading and ultra low cycle loading conditions. Razavi et al. (2017) had developed a new crack propagation blocking method, and carried out a test on crack initiation and propagation under cyclic loading. The test results showed that this approach is superior to the traditional single-plug method, and could greatly reduce the growth rate of fatigue cracks. Yang et al. (2019) proposed a new design detail for the local welded form of steel structure to improve the fracture behavior, and the FE fracture model of the connections was established by a quasi-static test. Qin et al. (2021) provided a modified continuous damage mechanics (CDM) model to predict the fatigue life for ULCF damage, which can reduce the relative error between the predicted fatigue life and the experimental fatigue life.

The above studies on the weld cracks mainly focus on the law of crack initiation and propagation, and the failure mechanism of fatigue damage. However, there are few studies on the influence of initial weld cracks on the seismic performance of steel beam-to-column connections, and the research related to initial weld cracks are mostly limited to some other fields such as aircrafts (Albedah et al., 2018; Citarella, 2009; Pokrovskii et al., 2018; Syed et al., 2014), ships (Babazadeh and Khedmati 2019; Yan and Huang 2015) and railways (Baptista et al., 2018; Ma et al., 2014; Xie et al., 2017). In this paper, the seismic performance of welded steel beam-to-column connections, which contain artificial-made initial surface notches in the welds of single beam flanges, were studied through experimental tests and finite element analysis.

2 Experimental Program

2.1 Experimental Purposes

The failure of steel structures under earthquakes is due to the phenomenons such as yield, local buckling, and weld fracture of structural members, which lead to the reduction of bearing capacity and stiffness of joints. This failure process is a cumulative damage failure process of ultra-low cycle fatigue. In this paper, full scale beam-column joints were designed for the experiment, focusing on the damage mechanism of weld joints in the structure. The influence factors such as test specimens, initial crack, material properties and loading protocol were considered, and the influence of weld damage and fracture on the seismic performance of joints was analyzed.

2.2 Test Specimens

Three full-scale specimens of steel beam-to-column connections—an H-shaped beam to H-shaped column (H-H) connection, an H-shaped beam to box column (H-B) connection, and a box beam to box column (B-B) connection—with initial cracks at the welds of the beam flanges and a specimen of the H-H connection without any initial cracks were prefabricated. All the specimens were in the same form of single-sided welded unreinforced flange-welded web (WUF-W) connections. For each specimen, the lengths of the beam and column were 1.5 m and 2.0 m, respectively.

The geometrical dimensions of the specimens are shown in Fig. 1. The linear stiffness ratios of beam to column of the specimens were almost the same, which were 0.51, 0.52, and 0.51 for that of the H–H connection, the H-B connection, and the B-B connection, respectively.

2.3 Details of the Initial Crack

In post-earthquake investigations, it is often found that brittle fractures occur in the bottom beam flange of steel beam-to-column connections due to welding defects. In most cases, the resulting crack caused by the welding defect at the bottom beam flange can be simplified into two types; the first is the surface notch along the length of the weld connecting a beam flange, and the other is the crack penetrating at the weld edge caused by non-permeable welding. Herein, a man-made surface notch as shown in Fig. 2, which is in the weld used to connect a column and a beam flange, was created during specimen prefabrication to simulate the first type of the cracks mentioned above. Then each specimen with this

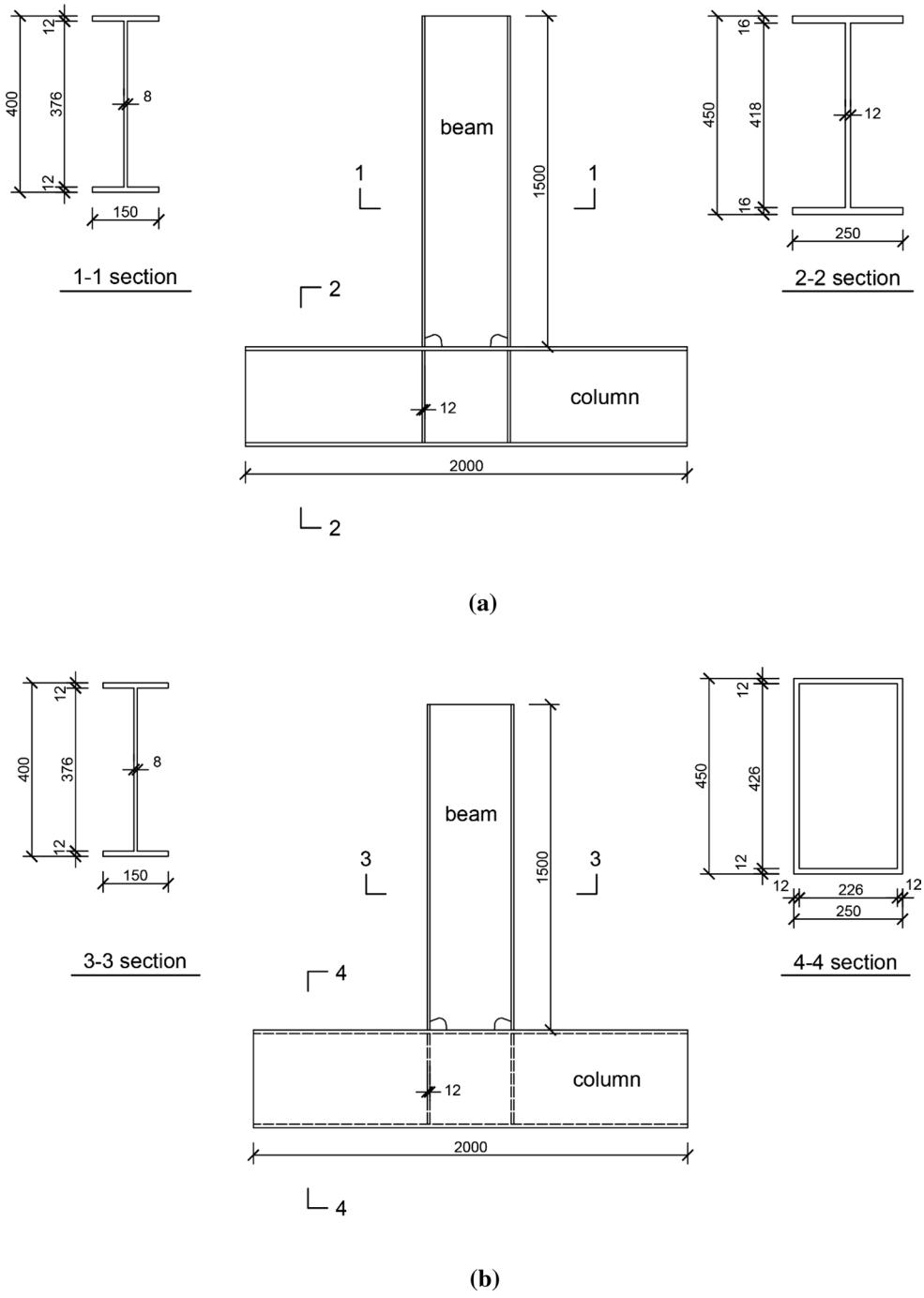

Fig. 1 Geometrical dimensions of specimens: **a** H–H connection, **b** H-B connection, **c** B-B connection, and **d** geometrical dimensions of weld hole

Fig. 1 (continued)

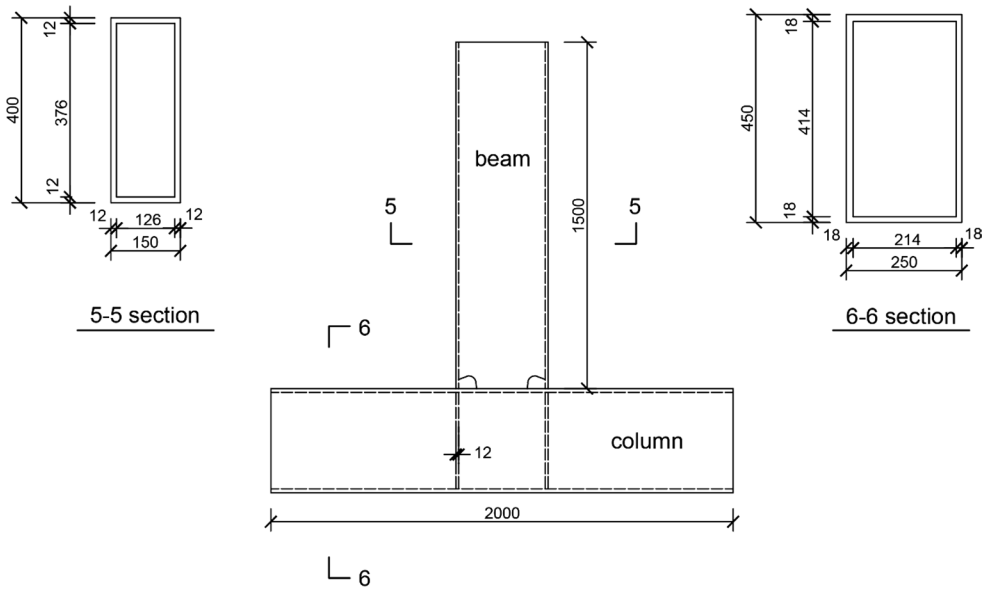

(c)

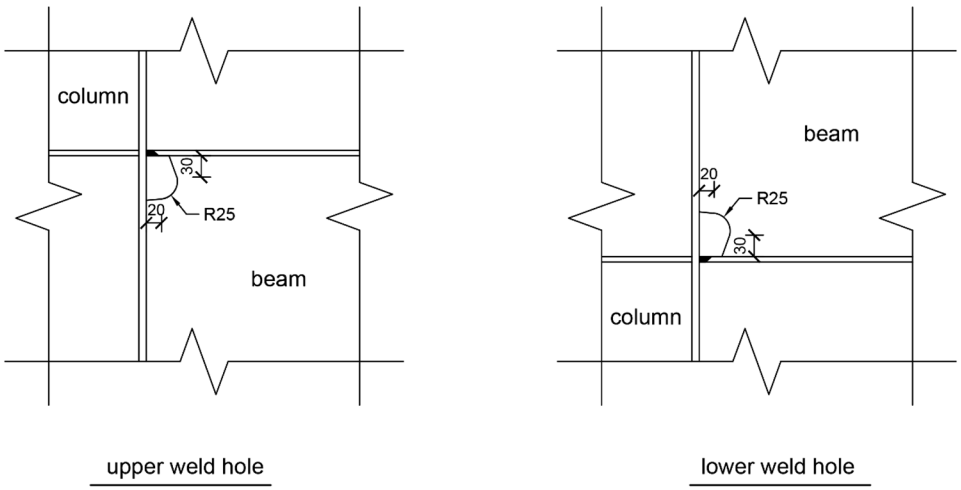

(d)

artificial crack was tested to explore the influence of the initial crack on the seismic performance of steel beam-to-column connections.

In practical engineering, the sizes of the initial crack at the weld vary along the beam flange width (eg., the crack depth in the middle of the weld length is always greater than that on the side). In order to apply the ductile fracture theory of microscopic materials to the macroscopic calculation of joint ductile fracture, the initial defect distribution of the flange of steel frame beam-column joints is assumed to be uniform, and the influence of the initial crack on the specific position of the flange is not considered. According to the equivalent penetrating crack conversion principle in elastic–plastic fracture mechanics, the defects such as slag inclusion and porosity at the weld site are converted into penetrating cracks on the undersurface of the beam flange. In addition, the error and uncertainty in the crack manufacturing process can be effectively reduced by this experimental design. A portable grinding machine was used to cut the weld of a single beam flange to obtain the initial crack. The crack produced by the machine was a surface-type crack in the middle of the weld height and uniformly distributed along the weld length (Fig. 3). The crack of each specimen was processed by the same cutting, and the depth and width

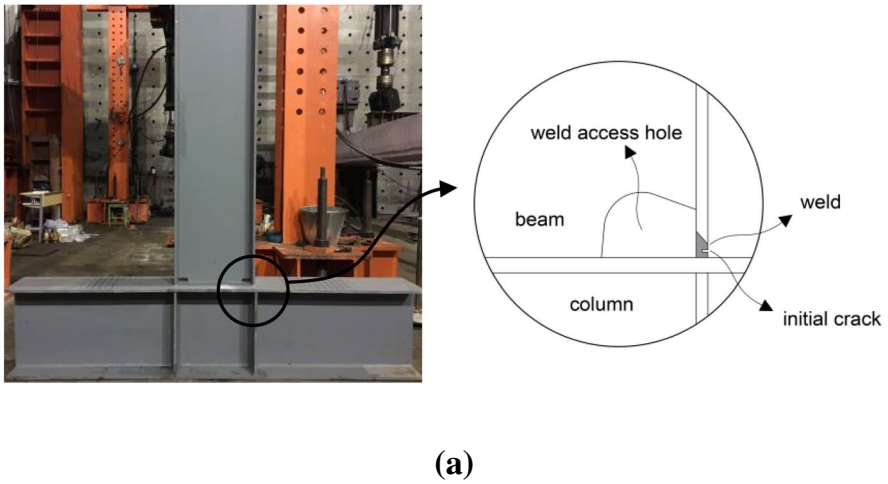

Fig. 2 Initial crack at the beam flange weld: **a** schematic diagram of the initial crack and **b** elevation view of the initial crack

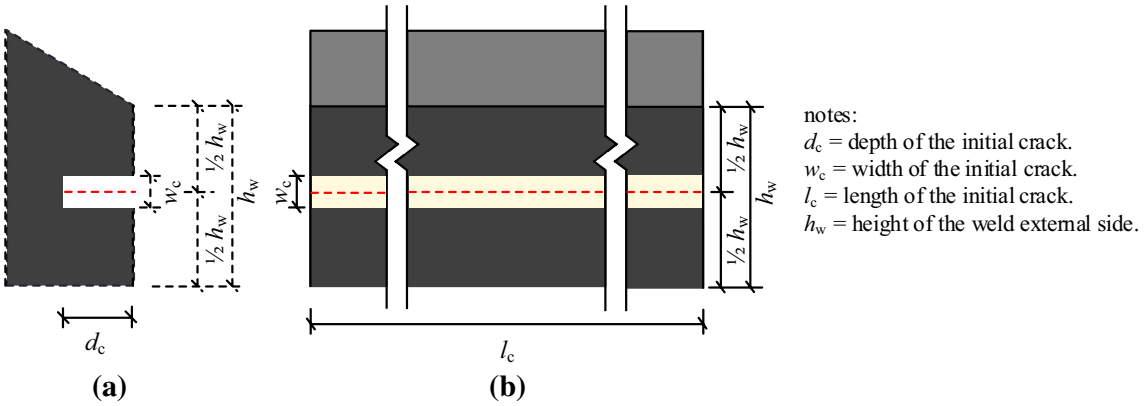

Fig. 3 Geometrical dimensions of the initial crack: **a** side view and **b** elevation view

of each crack were 1.0 mm and 0.5 mm, respectively, in order to obtain the crack propagation and connection failure modes of three kinds of beam-column joints under different initial conditions. To denote the experimental specimen, the name and characteristics of the specimen are shown in Table 1. According to the Welding Code for Steel Structures (GB50661-2011), grade I butt welds of steel structures shall be 100% flaw detection, and shall meet the requirements of no crack, no fusion, and no penetration. The single size of round defects such as porosity, slag, and tungsten in the

Table 1 Characteristics of the specimen

Specimen	Connection type	With or without initial crack
I	H–H	With
II	H–H	Without
III	H-B	With
IV	B-B	With

Table 2 Material properties

Material type	f_y (MPa)	f_u (MPa)
Q345 (16 mm)	392.7	548.2
Q345 (12 mm)	360.1	428.3
Q345 (8 mm)	353.8	479.6
E5015	391.4	615.8

weld shall be no more than 0.5 mm, and the total number of defects shall be 2–6. All the welds of each specimen were inspected by a full digital ultrasonic flaw detector before the experimental test, and the inspection results showed that there were no pores, slag inclusion, and other defects in the welds except the artificial cutting crack (if there are any).

2.4 Material Properties

The type of steel used for the beam and column of each specimen is Q345, and the type of weld metal is E5015. Coupon tests were carried out for these materials and the results are summarized in Table 2, where f_y and f_u are the yield strength and ultimate strength, respectively. The Young's Modulus and Poisson's ratio of all specimens measured in the test were 206 GPa and 0.3, respectively.

2.5 Test Setup

The general layout of the test setup is shown in Fig. 4. A hydraulic actuator with a maximum load capacity of 500 kN and a maximum available displacement stroke of 200 mm was employed to apply cyclic displacement loads on the experimental specimen. One end of the hydraulic actuator was fixed on a giant reaction wall, and the other end was connected to the beam end through four anchor rods and a fixed plate, which makes force transferred uniformly and smoothly. To simulate the axial pressure on the column of a frame structure, an axial force of 500 kN, which can be converted into an axial compression ratio of 0.18, was applied to one end of the column by another hydraulic actuator fixed on a reaction frame, while the other end of the column was pressed against to the reaction wall through a capping beam. Both ends of the column were fixed on the ground through a combination of a capping beam and prestressed anchor rods fixed to the ground, which restrains all the rotation and displacement of the column ends. In addition, lateral support, which was against an adjustable cylindrical bearing on the reaction frame on both sides, was provided below the loading position of the beam end to prevent lateral instability caused by out-of-plane torsion, displacement, or buckling.

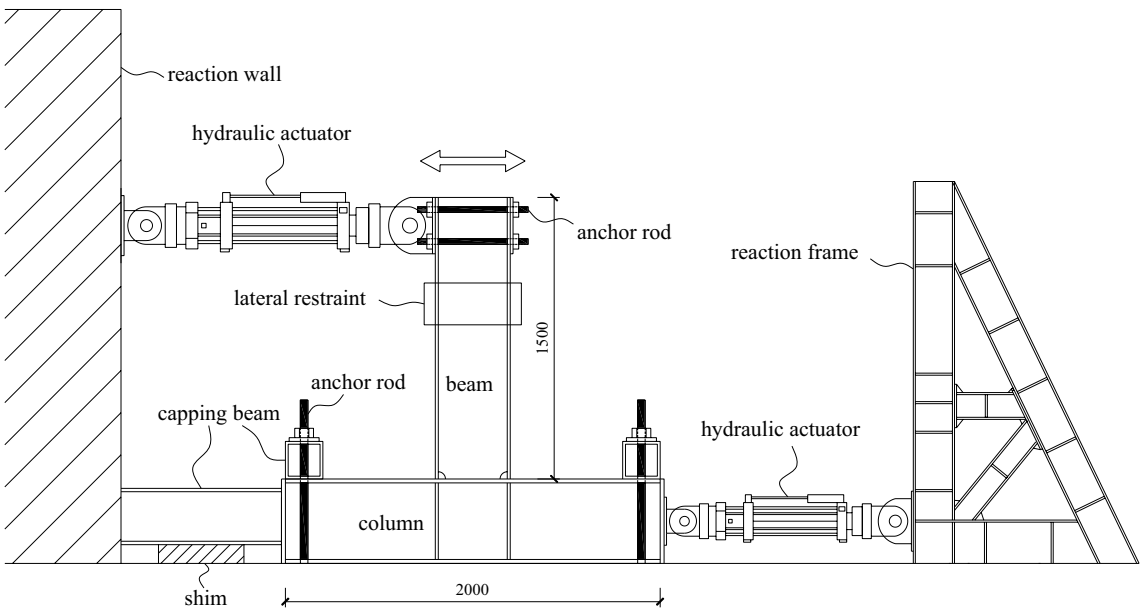

Fig. 4 Test setup

In this test, electronic automatic acquisition equipment was used to measure and collect the stress, strain, force, and deformation of the specimen. The computer was used to synchronize and automatically record them in real-time. The main measuring instruments included force transducer for servo actuator (50 T-MTS201.70), draw-wire displacement sensor, thimble displacement meter, and resistance strain gauge.

2.6 Loading Protocol

Incremental displacement loads were applied on the beam end for each specimen. The yield displacement of each specimen was estimated through preliminary finite element analysis. The results indicated that the yield displacements of H–H, B-H, and B-B joints were about 10 mm under the condition of 1 mm initial crack on the lower flange surface, so the minimum value of 10 mm was selected as the experimental standard. Since the connection with the initial crack is prone to fracture, the incremental magnitude of the displacement load should not be too large so as to ensure that the phenomena and results of the experimental test are more complete and elaborately recorded. The loading began with two cycles of 1/4 the yield displacement of Specimen IV (ie., 2.5 mm) for each specimen, followed by two cycles of multiples of 2.5 mm (ie., 2.5 mm, 5.0 mm, 7.5 mm, etc.) until failure or the limitation of the actuators. The loading procedure is illustrated in Fig. 5. It should be noted that it is in the positive direction of the displacement loading when the beam flange containing the initial crack (if there are any) is subjected to a tensile force.

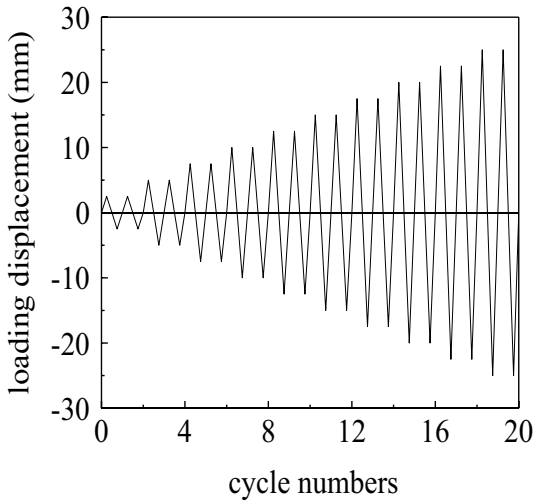

Fig. 5 Loading protocol

3 Experimental Results

3.1 Crack Propagation and Connection Failure Mode

To study the stress and strain changes in the weld zone of beam-column joints during the test loading process, instruments were arranged in the corresponding positions for real-time measurement. The data were processed and compared with ABAQUS finite element stress–strain curve to verify the stress development and distribution law. According to the feedback of the strain gauge in the test, when the loading displacement of the beam end was in the unyielding phase, the data measured by the sensor can be used basically. When the strain gauge exceeds the range, the strain data is gradually overloaded and presents a discrete phenomenon.

The crack propagation and the failure modes of each specimen under the action of the low cyclic displacement loads were observed in the experimental test. The stress distribution of joints was different under different structural types, but the development law was consistent. The stress concentration was obvious at the weld position of the flange of Specimen IV, so the crack of the B-B joint occurs first when the stress of upper and lower flanges along the weld direction reaches 352.7 Mpa. As the crack develops, the strain gauge exceeded the range and became overloaded. For Specimen I, a new crack that occurred during the 14th cycle appeared in the middle of the initial notch. Subsequently, the new crack spread along the path of the initial crack heading toward the two sides, and the initial crack was rapidly covered in the direction of the beam flange width. During the final cycle, the crack propagating trajectory suddenly deviated at both sides of the flange width and then the beam flange fractured there, as shown in Fig. 6a, possibly due to the influence of the residual stress at the welding toe.

For Specimen II, firstly a microcrack appeared at the junction of the beam flange surface during the 18th cycle and the weld access hole corner. As the amplitude of displacement loading gradually increased, it can be observed that the crack appeared on the other surface of the beam flange opposite to where it first appeared, indicating that the flange was penetrated by the crack in the direction of thickness. Then the beam flange was gradually torn along the width direction and finally fractured. The fracture surface of Specimen II was roughly aligned with the corner of the weld access hole in the horizontal direction (Fig. 6b).

The new cracks of Specimens III and IV both appeared in the middle of the initial crack notch before the 10th cycle, which was the same place as observed in Specimen I. Then the cracks quickly spread along the path of the

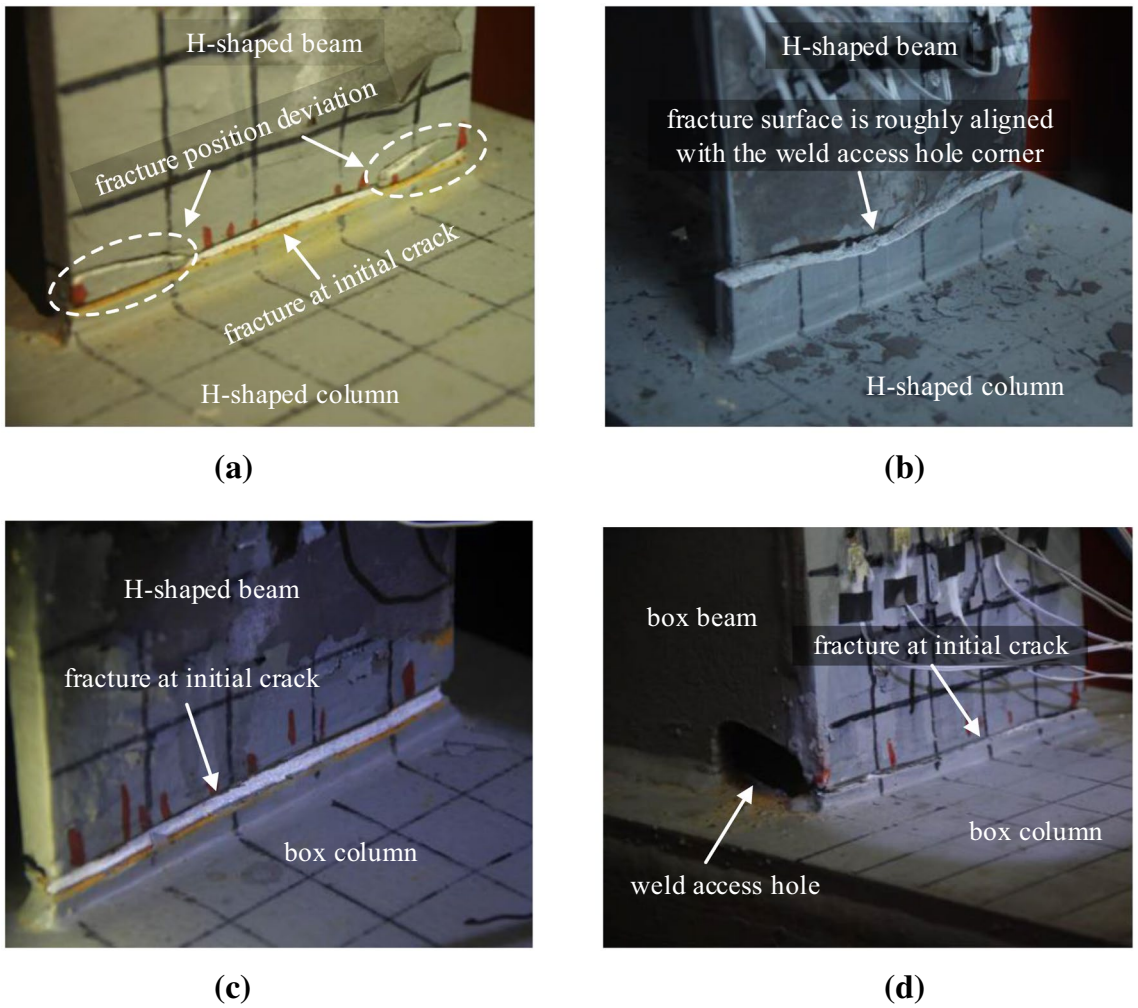

Fig. 6 Fracture position at the beam flange: **a** Specimen I, **b** Specimen II, **c** Specimen III, and **d** Specimen IV

initial crack and gradually extended into the weld. Finally, the beam flanges with the initial crack were penetrated by the spreading new cracks and fractured as shown in Figs. 6c, d for Specimens III and IV, respectively. The crack propagation of Specimens III and IV was similar to that of Specimen I except for having no crack deviation. It can be concluded that the crack propagation and fracture position of the steel beam-to-column connection will be significantly changed if there is an initial crack existing in the beam flange weld.

The main process of crack propagation, the corresponding cycle number (n), and loading displacement amplitude (D) are summarized in Table 3, where "crack appearing" means that the new crack appears during loading; "penetrating or covering" means the new crack penetrates the beam flange in the direction of thickness for Specimen II, or the initial crack

Table 3 Summssary of the experimental test results

Specimen	Crack appearing		Penetrating or covering		Flange fracture		K_i (kN/mm)	F_y (kN)	δ_y (mm)	F_u (kN)	δ_u (mm)	μ
	n	Δ (mm)	n	Δ (mm)	n	Δ (mm)						
I	14	17.5	18	22.5	20	25.0	12.30	178.7	12.0	263.0	25.0	2.1
II	18	22.5	22	27.5	26	32.5	12.28	177.4	12.1	287.5	33.8	2.8
III	9	12.5	11	15.0	14	17.5	16.89	185.7	12.0	236.0	17.3	1.4
IV	7	10.0	9	12.5	12	15.0	16.72	189.7	11.9	227.9	14.9	1.3

is covered in the direction of beam flange width by the new crack for Specimens I, III, and IV; "flange fracture" means the beam flange fractures caused by the crack propagation, that is, the specimen failure. The failure process of the test specimens is roughly in the following stages. Firstly, micro-cracks appear in local positions. Then the cracks continuously deepen and expand until they develop into penetrating cracks. Finally, fracture failure occurs in the test specimens with sudden noise. The cycle number and displacement amplitude at each crack propagation stage of Specimen I are less than those of Specimen II, and Specimen I had only 6 cycles from new crack appearance to specimen failure, which is 2 cycles less than that of Specimen II, indicating that the crack propagation of Specimen I developed earlier and faster than that of Specimen II. It can be concluded that under repeated loading, the initial crack at the weld of a single beam flange not only changes the crack propagation mode, but also accelerates the speed of crack initiation and propagation, and reduces the structural ductility. Among all the specimens with the initial crack, Specimen IV was the first to have new crack initiation and fracture, followed by Specimen III, and the last was Specimen I. This shows that although the crack propagation modes of Specimens I, III, and IV are similar, their developing rates differ a lot.

3.2 Hysteretic Behavior

Figure 7 plots the hysteresis and skeleton curves of the experimental specimens. Specimen II had full hysteresis loops and a good energy dissipation capacity, while Specimen I, III, and IV showed flat hysteresis curves with a small area of hysteretic loops and a poor energy dissipation capacity, due to the presence of the initial crack. By comparing the hysteresis curves of Specimens I, III and IV, it can be found that the hysteretic properties of different connections with the initial crack are significantly different; Specimen I had the most hysteretic cycles and the largest hysteresis loop area, followed by Specimen III, while the last was Specimen

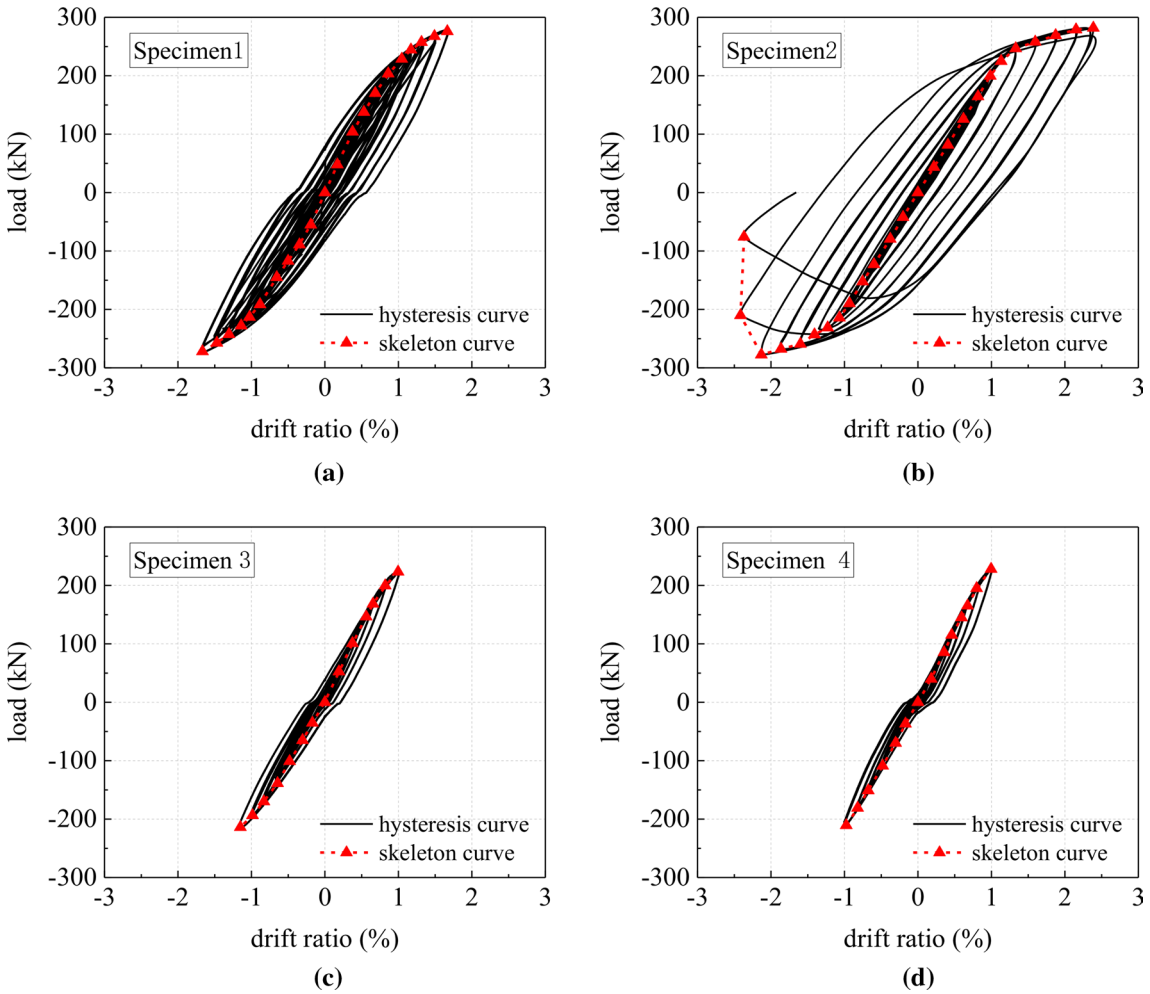

Fig. 7 Hysteresis and skeleton curves: **a** Specimen I, **b** Specimen II, **c** Specimen III, and **d** Specimen IV

IV. As for the skeleton curve, Specimen II had the complete stages of elasticity, elastoplasticity, and strength degradation, while Specimen I had only the stages of elasticity and unabiding elastoplasticity before failure. The skeleton curves of Specimens III and IV were broken off when they just enter the elastoplastic stage, which shows the characteristic of brittle failure.

The results of the initial stiffness (K_i), yield strength (F_y), ultimate strength (F_u), yield displacement (δ_y), ultimate displacement (δ_u) and ductility coefficient (μ) of the experimental specimens are shown in Table 3, and the ductility coefficient (μ) can be calculated as follows.

$$\mu = \delta_u/\delta_y \tag{1}$$

The initial stiffness, yield strength, and displacement of Specimen I are almost the same as those of Specimen II, but the ultimate strength, displacement, and ductility coefficient decreases by 8.5%, 26.0%, and 25.0%, respectively, indicating that the presence of the initial crack would weaken the ultimate strength of the H–H connection, and significantly reduce the ultimate deformation and ductility. By comparing the results of Specimen I, III, and IV, it can be seen that although the yield strength of Specimen I is slightly lower, its ultimate strength is 10.3% and 13.3% higher than that of Specimens III and IV, respectively. The yield displacements of the three specimens are basically the same. However, the ultimate displacements of Specimen III and IV are reduced by 30.8% and 40.4%, respectively when compared with that of Specimen I, and it results in the reduction of ductility coefficient by 33.3% and 38.1%, respectively. It can be concluded that the ultimate displacement and ductility of the connections with box columns are significantly less than those of the connections with H-shaped columns, which can be inferred that the box column has a greater restraint on the deformation of the beam resulting in a reduction on structural ductility.

4 Finite Element Analysis

4.1 Modeling Approach

The extended finite element method (XFEM) was proposed by Belytschko and Black in 1999, which can be used to simulate the crack propagation (Belytschko & Black, 1999; Belytschko et al., 2003). This method can improve the element shape function to adapt to the discontinuity of elements so that the mesh can be generated completely according to the structure shape, and there is no need to remesh when modelling the crack. The XFEM can separate the mesh boundary of the crack model from that of the conventional model part, and the crack model can be meshed separately and regularly without considering the crack tip size. This is because that a particular asymptotic field function of the crack tip is adapted to reflect the stress singularity characteristics in the crack tip region without dividing high-density meshes. Therefore, the XFEM greatly simplifies the meshing and reduces the computational resources, so as to easily simulate the three-dimensional (3D) finite element model with crack propagation.

Four 3D finite element models of the steel beam-to-column connections with the initial crack were established in ABAQUS software, and the initial crack at the weld was simulated through the function of Seam Crack in the XFEM module. The maximum principal stress theory was used as the damage criterion. In details of the damage parameter setting, the energy criterion was adopted for the damage evolution, the softening mode was set to linear, and the degradation mode was set to maximum degradation. Then the power law was employed for the mixed-mode behavior, and the power parameter was set to 1. In addition, the energy model was adopted in the model mix ratio, and the damage stability parameter was set as 1×10^{-5} to ensure good convergence in the calculation.

The material nonlinearity was considered during the analysis by adopting a bilinear stress–strain relation as that in Table 1. The weld model was not established separately, but included in the steel beam model, and the weld was simulated by partition and material attribute assignment. A shell model of the initial crack was embedded into the weld part of the bottom beam flange, and the embedding position was the same as that in the experimental specimen. 8-node and hexahedral reduced (C3D8R) elements were used for the beam, column, and weld of the finite element model, while 4-node reduced integration (S4R) elements were adopted for the initial crack model in the weld. The mesh was refined in the elements which are in the vicinity of the weld to obtain more accurate calculation results. Take the meshing for Specimen I as an example, and the meshing result is shown in Fig. 8. The von Mises yield criterion of ABAQUS is adopted in the damage process, which is a mixed model of isotropic and follow-up strengthening. Then, a nonlinear full Newton–Raphson direct method was used for the analysis. Increment step size was set to automatic to be controlled by the program. All the degrees of freedom were restrained at one end of the column, and an axial force of 500 kN was applied to the other end, which was restrained for the remaining degrees of freedom. The cross-section of the beam end in the loading position was coupled to a reference point and then the cyclic displacement load used in the experimental test was applied to the reference point. In addition, the factor of welding residual stress was not considered in the finite element analysis.

The mesh of weld position was set as 0.5, 1.0, 1.5, 2.0, and 2.5 respectively, and then the changes under fatigue

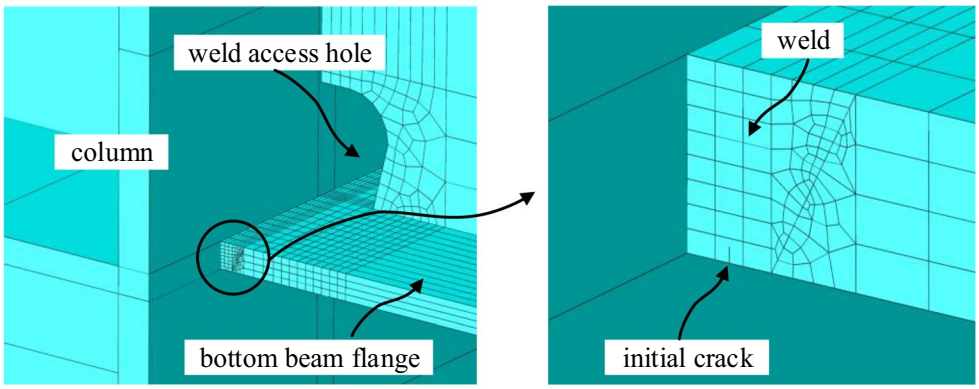

Fig. 8 Meshing for the finite element model

load were compared. According to the sensitivity analysis of macroscopic crack length and element size, the mesh size of weld position was determined to be set as 1.5 mm.

5 Results and Comparison with Experimental Test

Figure 9 shows the failure mode of each specimen in the finite element analysis. The fracture positions were almost the same as those of the experimental test as shown in Fig. 6, that is, Specimen I, III, and IV all fractured at the location of the initial crack, while Specimen II fractured at the steel beam flange with a fracture surface aligned with the weld access hole corner.

Figure 10 shows the comparison of the hysteresis curve results between the finite element model and experimental test. The hysteresis curves of the experimental Specimens I, III and IV show a pinching slip near the zero coordinates. This is due to the fact that the initial crack formed by artificial cutting has a width of 0.5 mm, and it is cannot be ignored in the experimental test. When the applied load returns to zero, only a small force is needed to close the crack while a large displacement is occurred, which leads to a slip as the experimental results indicate. However, the initial crack in the finite element model is a two-dimensional surface without a width, and this phenomenon of slipping does not occur. In addition, although the cycle numbers of some finite element curves are slightly different from those of the experimental test curves (ie., the finite element curve of Specimen I is reduced by 1 cycle, and that of Specimen II is reduced by 2 cycles), the hysteretic curve of the finite element model is still in good agreement with the experimental test curve. It can be concluded that the XFEM can effectively simulate the crack propagation and the hysteretic behavior of the connection under low cyclic loads.

6 Influence of the Initial Crack

6.1 Hysteretic Behavior and Failure Mode

Existing pieces of literature (Joh & Chen, 1999; Xu & Ellingwood, 2011) have shown that the size of cracks has a great impact on structural performance, thus the uncertainty of the initial crack size cannot be ignored. Herein, the depth of the initial crack (d_c) was set as 0, 1, 2, and 3 mm, respectively, to discuss the effect of different initial crack depths on the seismic performance of the beam-to-column connection through finite element analysis. The type and geometric dimensions of the beam-to-column connections, and the initial crack position remain the same as aforementioned. Herein, the connections are denoted in the form of A-b, where A means the connection type, and b means the depth of the initial crack (eg., HB-2 refers to the H-B connection with an initial crack depth of 2 mm).

Figure 11 shows the hysteresis curves and failure modes of the connections with different initial crack depths. For the connections without the initial crack, HH-0 has the largest number of hysteresis cycles and maximum hysteresis loop area, which indicates HH-0 has the best hysteretic performance among the three types of the connections without the initial cracks, followed by HB-0, and BB-0 has the worst hysteretic performance with a maximum displacement being only half of that of HH-0, showing brittle failure. It can be seen that the number of hysteresis cycles of each connection decreases gradually with the increase of initial crack depth. The relation between the cycle number of each connection and the initial crack depth is plotted in Fig. 12. The H-H connection has the maximum cycle number among the three types of connections no matter what the initial crack depth is. For the H-B and B-B connections, when the initial crack depth is no more than 2 mm, the B-B connection has the lower cycle number, while when the initial crack depth is 3 mm, the

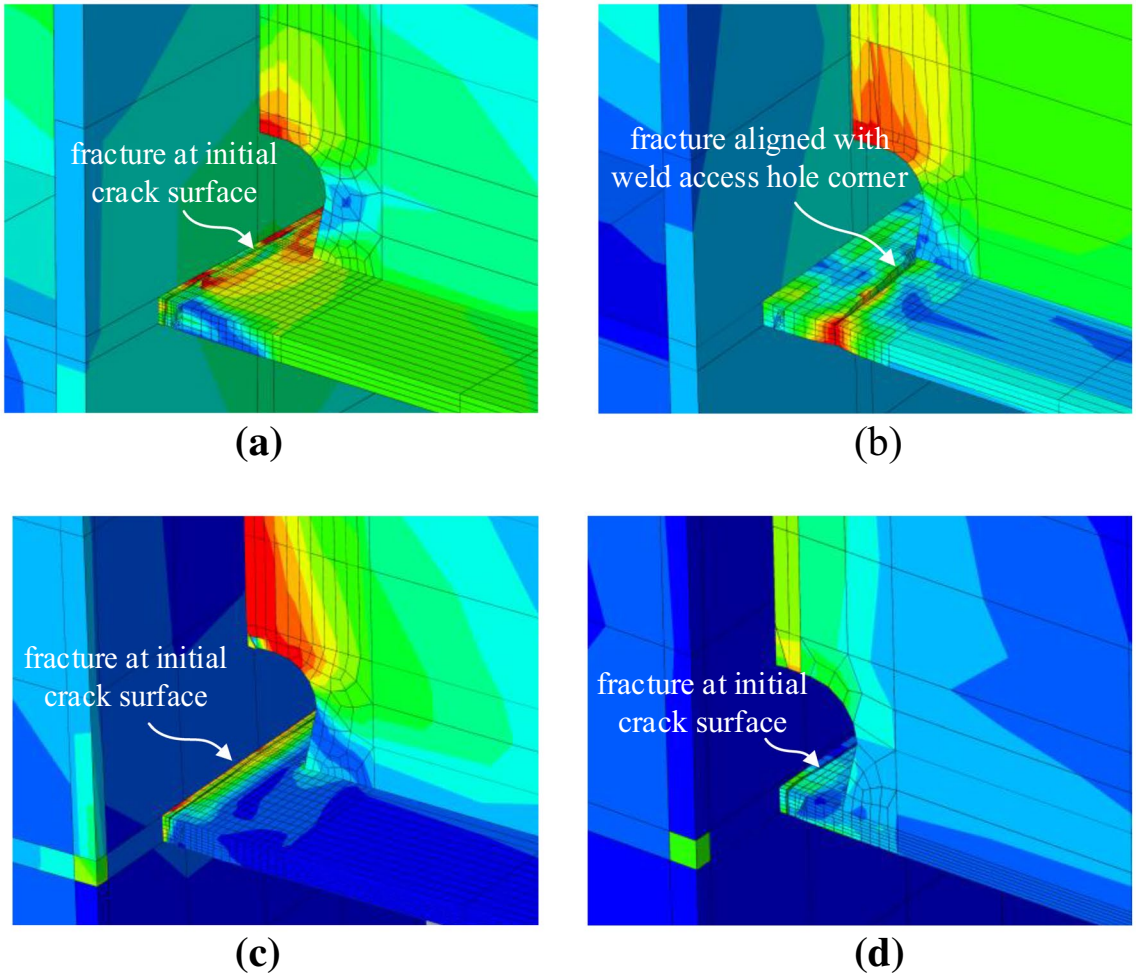

Fig. 9 The fracture mode of the FE model: **a** Specimen I, **b** Specimen II, **c** Specimen III, and **d** Specimen IV

B-B connection has more cycles than the H-B connection. In general, although B-B connections do not have many hysteresis cycles in the case of different crack depths, the cycle number of them decreases the least within the range of 0 to 3 mm crack depth, which indicates that the hysteretic performance of the B-B connection is the least insensitive to the initial crack depth.

It can also be concluded from Fig. 11 that the presence of the initial crack at the weld has a great influence on the fracture positions of the H-H and H-B connections. The fracture positions of HH-0 and HB-0 were aligned with the weld access hole corner, while BB-0 fractured at the weld of the beam end due to the maximum stress there; the remaining specimens all fractured at the location of the initial crack, and the initial cracks with different depths do not change the fracture position because these connections have stress concentration at their initial crack tips no matter how long the crack depths are, and when the stress exceeds the maximum principal stress, the crack will be opened and expanded to specimen fracture.

The bearing strength and deformation capacities of the specimens are shown in Table 4. In general, the results of the specimens with the same connection type show a decreasing trend with the increase of the initial crack depth. Except for HH-0, HB-0, and BB-0, the properties of the specimens are generally asymmetric in two directions; the yield strength and displacement, and ultimate strength of these specimens are lower when the loading direction is positive. This is because, during the positive loading, the initial crack at the weld of the single beam flange is opened, which results in the seismic performance of the connection being reduced; when the specimen is negatively loaded the crack is closed, which has little impact on the connection performance.

The relation between the positive ultimate strength of the specimen and the initial crack depth is plotted in Fig. 13. It can be seen from Table 4 that the presence or absence of initial cracks has a significant impact on the strength degradation of joints. The ultimate bearing capacity of the joints with initial cracks decreases about 22% under reciprocating load. When the initial crack depth is less than 2 mm, the

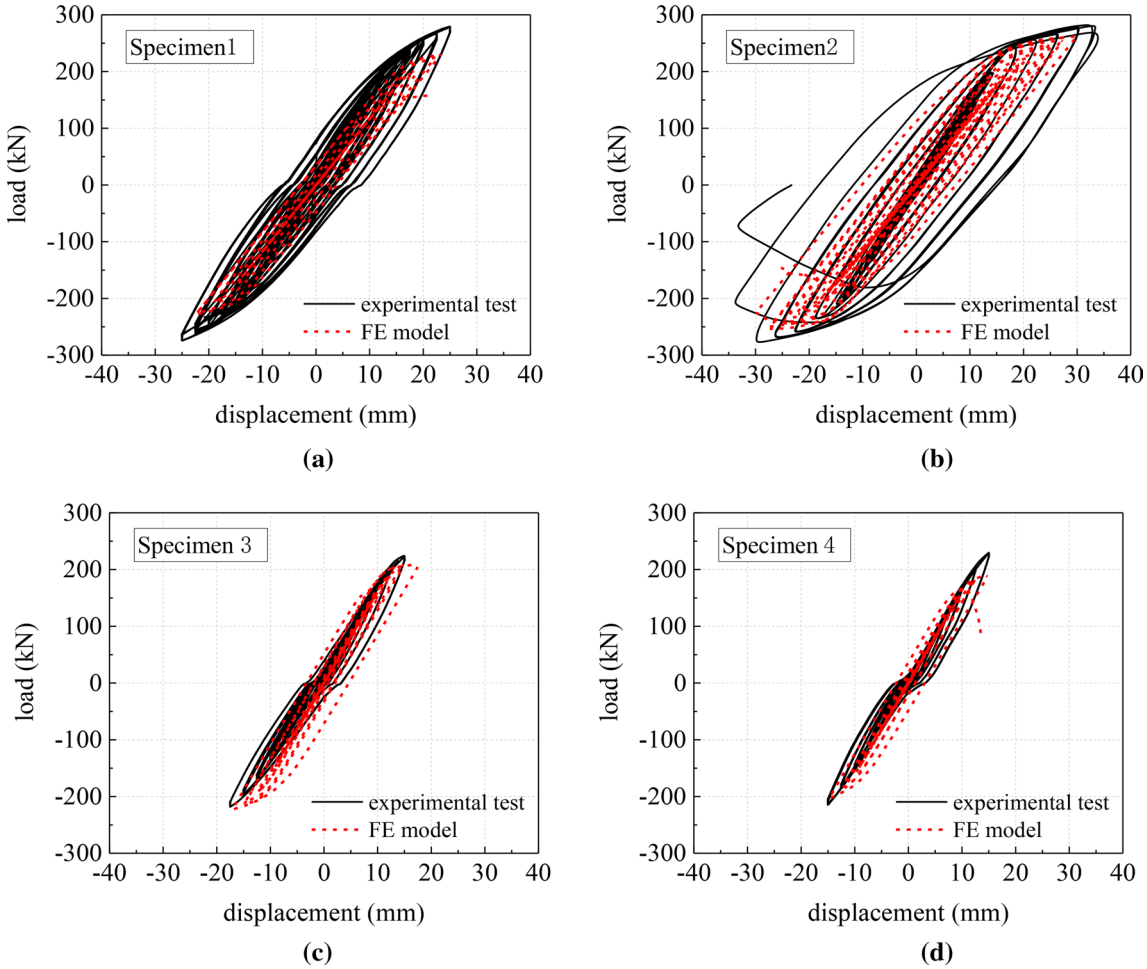

Fig. 10 Comparison of the hysteresis curves between the FE model and experimental test: **a** Specimen I, **b** Specimen II, **c** Specimen III, and **d** Specimen IV

H-H connection has the maximum ultimate strength, followed by the H-B connection, and the last is the B-B connection. However, the ranking result is different when the initial crack depth is 3 mm; the ultimate strength of the B-B and H-H connections is both 41.15 kN higher than that of the H-B connection.

According to the specification for a seismic test of buildings (JGJ/T 101-2015 2015), the structural failure load should be taken as 85% of the ultimate strength of specimens. Through interpolation calculation, the ultimate strength value, which is equivalent to 85% of the ultimate strength of the specimen without initial crack, is marked in Fig. 13. According to the interpolation calculation results, when the initial crack depths of the H-H, H-B, and B-B connections are 1.26, 1.63, and 2.59 mm, respectively, the connection fails due to insufficient maximum strength bearing capacity. It can be seen that the increase of the initial crack depth has a great impact on the ultimate strength bearing capacity of H-H and H-B connections. In practical engineering, the welding quality of steel beam-to-column connections, especially the H-H and H-B connections, should be ensured during the welding construction process. After earthquakes, it is necessary to monitor and check the crack size in time to ensure that the strength bearing and deformation capacities of beam-to-column connections meeting the requirements.

6.2 Strength Degradation

The strength degradation of steel beam-to-column connections is caused by the plastic development of structural components and continuous crack propagation. The strength degradation coefficient (λ) can be calculated as followed.

$$\lambda = \frac{F_{\mathrm{P}} - F_{\mathrm{c}}}{F_{\mathrm{P}}} \tag{2}$$

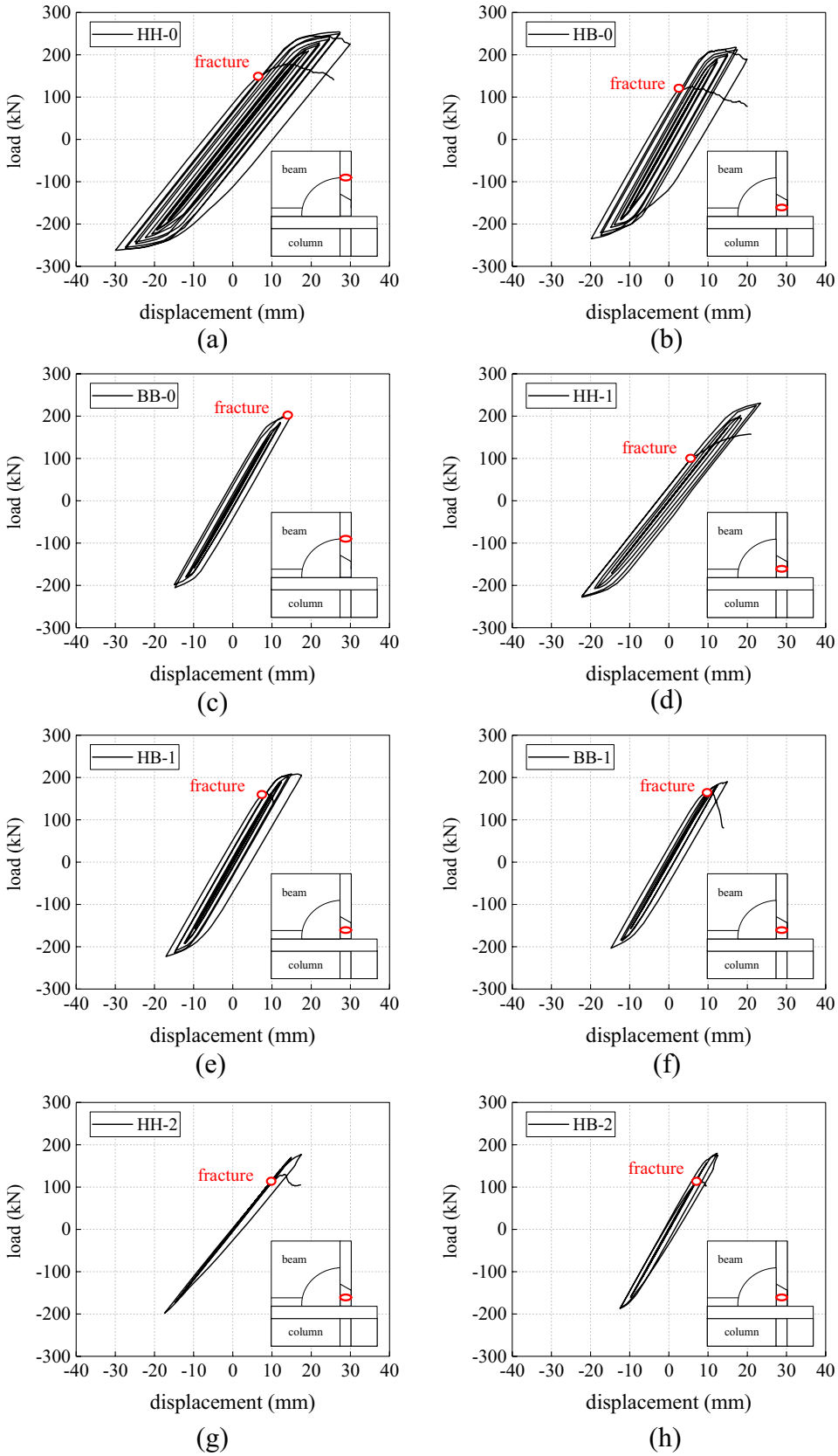

Fig. 11 Hysteresis curve and failure mode: **a** HH-0, **b** HB-0, **c** BB-0, **d** HH-1, **e** HB-1, **f** BB-1, **g** HH-2, **h** HB-2, **i** BB-2, **j** HH-3, **k** HB-3 and **l** BB-3

Fig. 11 (continued)

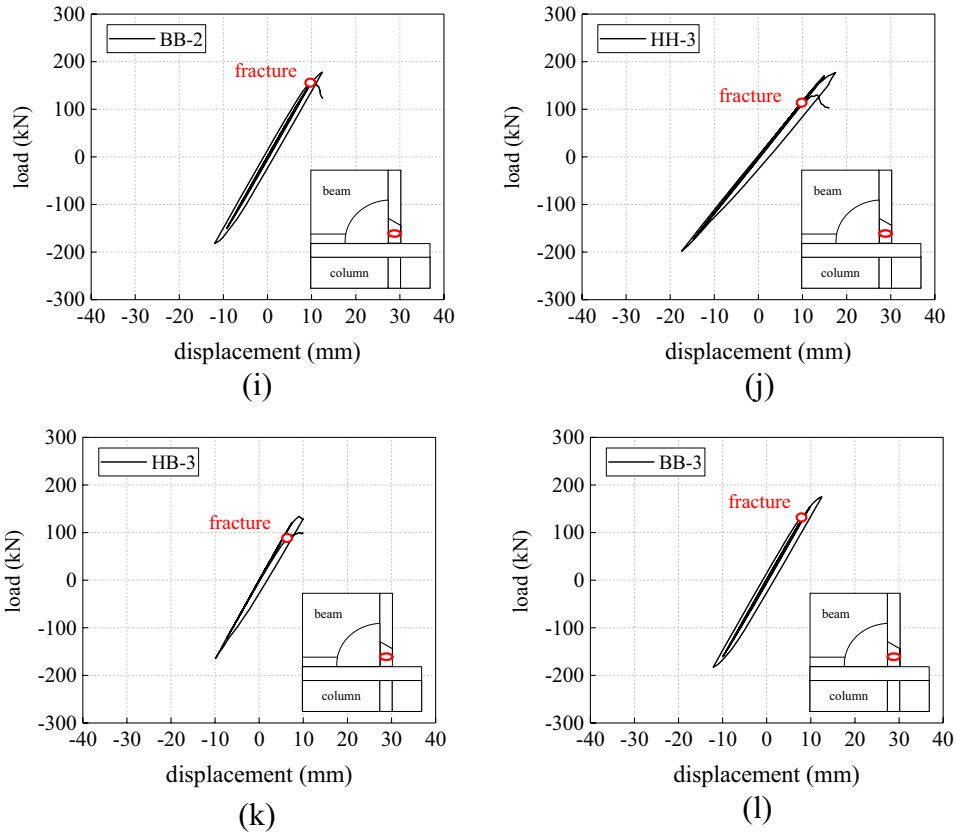

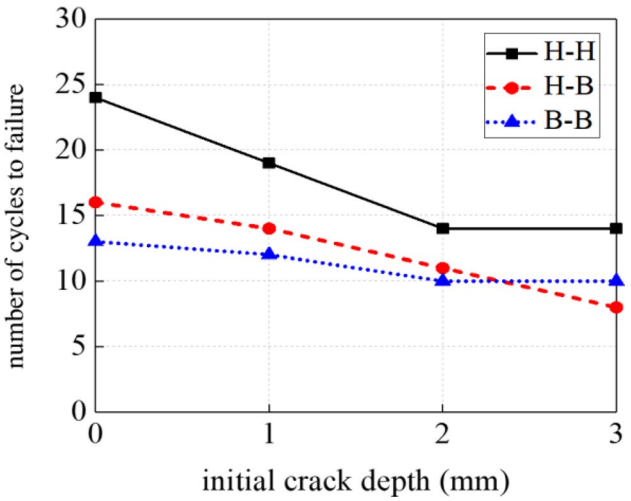

Fig. 12 Relation between the number of cycles to failure and initial crack depth

where F_P is the strength bearing capacity corresponding to monotonic loading; F_c is the strength bearing capacity corresponding to cyclic loading.

Figure 14 shows the relation between the strength degradation coefficient and the cycle number of each specimen, and the sign of the x-axis reflects the loading direction. The specimens of HH-0, HB-0, and BB-0 have little strength degradation when the cycle number is not large, but at the late loading stage, the strength degradation coefficients of the three specimens without the initial crack increase sharply due to the crack propagation, and show obvious asymmetry in different directions. For the H-H connection with the initial crack, their strength degradation coefficient is 0 at the primary stage, then they increase abruptly for the first time. After the sudden increase, the curves begin to decrease and then rise again until the last few cycles. The strength degradation coefficient curves generally present a trend of rising-descending-rising. The reason for the first rise is that the H-H connections crack preferentially under cyclic loading, resulting in strength degradation. Subsequently, due to the cracking of the connections under monotonic loading, the strength degradation coefficients decrease. Finally, under cyclic loading, the strength degradation coefficients near the connection failure increase again as it enters the stable degradation stage, which is consistent with the hysteresis effect of crack growth. Although the strength degradation coefficient curves of the H-B connections are similar to those of the H-H connections, the ranges of their degradation coefficient values are relatively limited. The strength degradation coefficients of the B-B connections are low at the initial stage of loading. Then their positive curves

Table 4 Results of FE analysis

Connection	d_c (mm)	Direction	Ki (kN/mm)	Fy (kN)	δ_y (mm)	F_u (kN)	δ_u (mm)	μ
H–H	0	Positive	11.73	176.71	17.26	252.35	29.95	1.74
		Negative	11.73	179.36	16.76	258.85	29.74	1.77
	1	Positive	11.71	160.34	14.75	224.19	22.20	1.51
		Negative	11.73	160.42	15.27	228.52	23.04	1.51
	2	Positive	11.71	130.14	11.70	174.37	17.38	1.49
		Negative	11.73	147.79	13.22	196.03	17.59	1.33
	3	Positive	11.71	129.36	11.41	172.20	17.17	1.51
		Negative	11.73	147.59	13.20	196.02	17.57	1.33
H-B	0	Positive	16.66	147.46	11.86	221.19	19.90	1.68
		Negative	16.66	159.73	11.53	245.02	19.90	1.73
	1	Positive	16.64	138.34	9.03	203.86	14.66	1.62
		Negative	16.65	144.44	9.37	210.36	14.87	1.59
	2	Positive	16.64	130.98	8.09	178.70	12.36	1.53
		Negative	16.67	136.40	8.92	185.20	12.36	1.39
	3	Positive	16.57	95.13	6.12	131.05	9.92	1.62
		Negative	16.66	125.11	7.59	163.54	9.92	1.31
B-B	0	Positive	16.45	142.63	9.59	204.69	15.08	1.57
		Negative	16.45	144.39	9.62	202.53	14.66	1.52
	1	Positive	16.44	134.11	8.84	187.37	14.66	1.66
		Negative	16.45	142.04	9.22	200.53	14.47	1.57
	2	Positive	16.41	129.28	8.56	176.53	12.36	1.44
		Negative	16.44	134.49	8.81	183.03	12.15	1.38
	3	Positive	16.41	124.33	8.13	172.20	12.15	1.49
		Negative	16.45	132.40	8.55	180.87	12.15	1.42

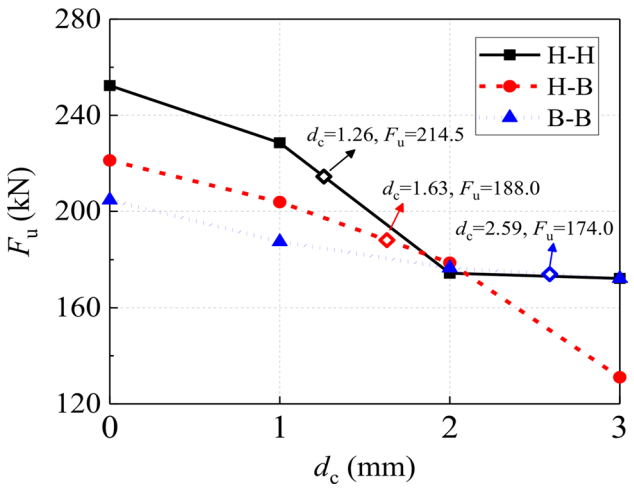

Fig. 13 The relation curve of the positive ultimate load and initial crack depth

increase sharply during the last few cycles, while the negative curves are asymmetric and the increase is modest.

It can be concluded that the larger the initial crack depth is, the greater the strength degradation is and the earlier it occurs. Moreover, the strength degradation of the H-H connection under cyclic loading is the most sensitive to the initial crack, followed by that of the H-B connection. Although the B-B connection has obvious brittle failure characteristics, its strength degradation is the least affected by the initial crack, because no matter whether the B-B connection contains the initial crack or not, it is very low except for the sharp increase in the late loading stage near the fracture.

6.3 Dissipated Energy

Figure 15 shows the dissipated energy of each specimen under the action of the low cyclic loading. When there is no initial crack, the energy dissipation of the H–H connection is 2.27 and 3.73 times that of the H-B and B-B connections, respectively. With the increase of the initial crack depth from 0 to 1 mm, the dissipated energy of all specimens decreases sharply, which is particularly obvious in the H-H connection. As the initial crack depth increases from 0 to 1 mm, the dissipated energy of the H-H connection decreases by 67.1%, and when the initial crack depth increases from 2 to 3 mm, the dissipated energy decreases by only 8.4%, which indicates that the energy dissipation capacity of the H-H connection is very sensitive to the initial crack with a smaller depth. In addition, although the energy dissipation of the H-B connection is 64.7% higher than that of the

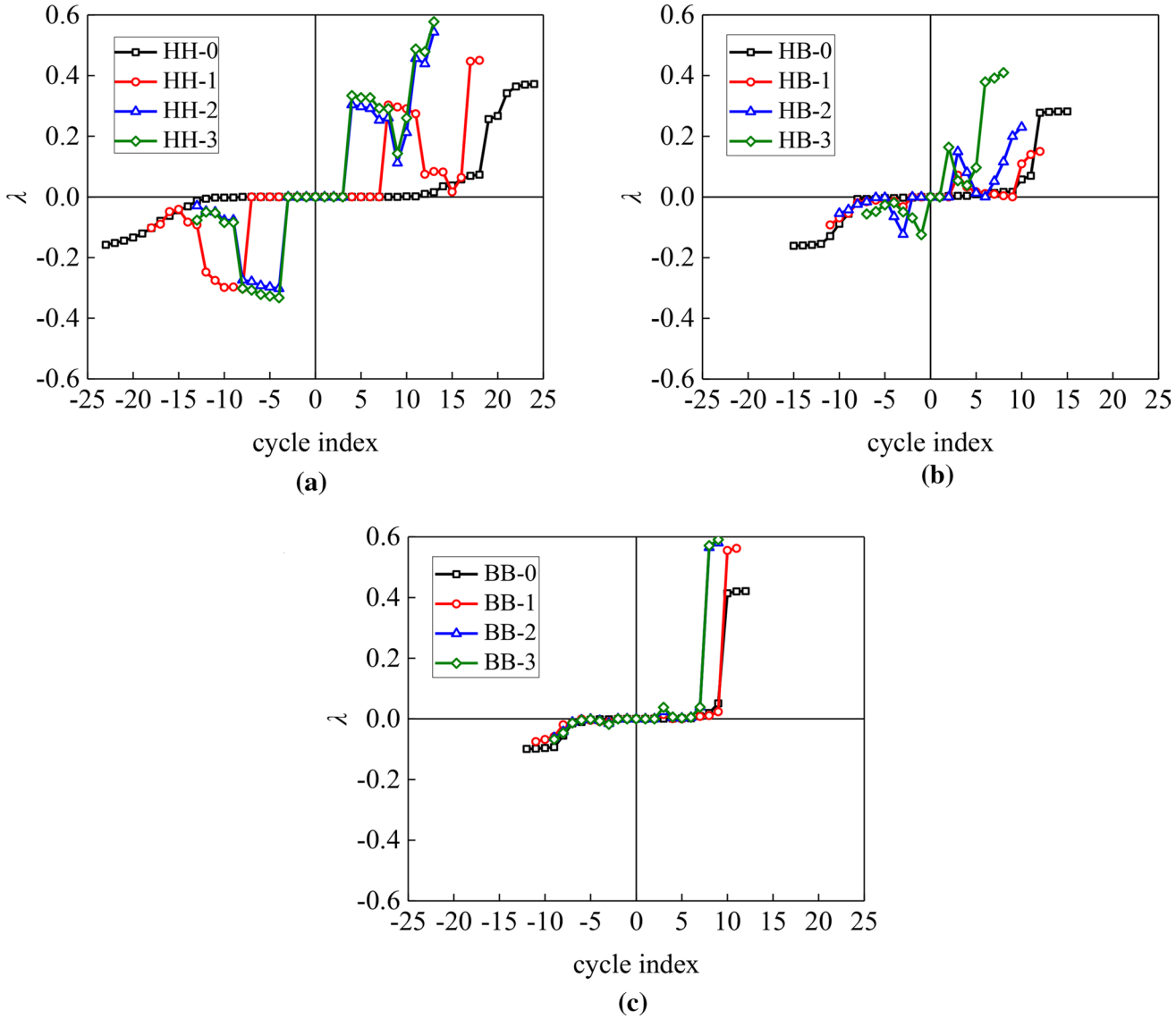

Fig. 14 Strength degradation coefficient: **a** H–H connection, **b** H-B connection, and **c** B-B connection

B-B connection when there is no initial crack, the dissipated energy of the H-B connection becomes almost the same when the initial crack depth is 2 and 3 mm, which indicates that the initial crack depth has less influence on the energy dissipation capacity of the B-B connection.

7 Conclusion

To investigate the influence of initial surface notches caused by welding defects on the seismic performance of welded steel beam-to-column connections, three experimental specimens with the same artificial cracks and different connection types (the H-H, H-B, and B-B connections) as well as a specimen (the H-H connection) without any initial cracks were tested. Through the XFEM in ABAQUS software, the influence of the depth of the initial crack on the seismic performance of these connections was discussed by comparing the hysteretic behaviors, failure modes, strength degradation, and energy dissipation. It is assumed that the initial crack spreads along the weld of a beam flange and its cross-sectional size remains the same along the weld length to facilitate the operation and reduce errors during the crack manufacturing process. The factors of the location and size of the initial crack are not considered during the research and these limitations are worth to be optimized in future studies.

It can be concluded that the crack propagation and fracture modes of welded steel H-H and H-B connections will be significantly changed if there is an initial crack existing in the weld of a single beam flange. In detail, connections

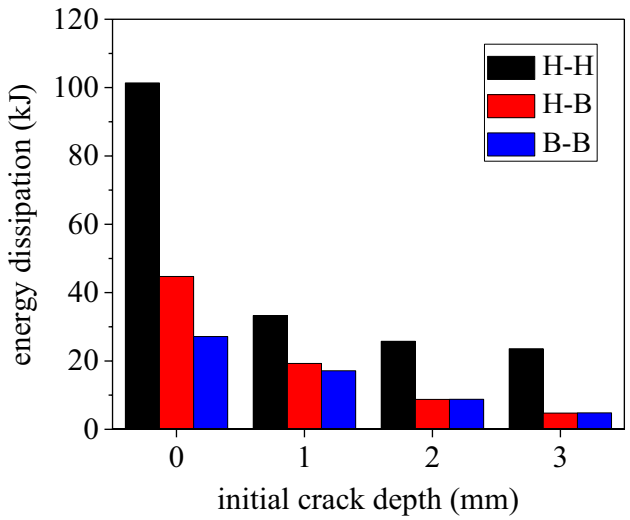

Fig. 15 Relation between the dissipated energy and initial crack depth

with the initial crack will crack at initial crack notches and fracture there regardless of the depth of the initial crack and connection types. As for H-H and H-B connections without any initial cracks, the crack and fracture occur in the location of the beam flange where is aligned with the weld access hole corner, while B-B connections without initial cracks fracture at the welds of beam flanges due to large stress there, which is the same as the case with the initial crack.

The initial stiffness of connections is scarcely affected by the initial crack, while the ultimate strength, deformation, ductility, and energy dissipation are significantly reduced, and these hysteretic behaviors are asymmetric in two loading directions due to the presence of the initial crack. When there is no initial crack, the hysteretic performance, ultimate displacement, and ductility of connections with box columns are significantly less than those of connections with H-shaped columns, indicating brittle failure in B-B connections.

Among the three different connection types, the seismic performance of H-H connections is the most sensitive to the depth of the initial crack, followed by that of H-B connections, and the depth of38the initial crack has less influence on the seismic performance of B-B connections. As a result, the weld quality of steel beam-to-column connections especially the H-H and H-B connections should be carefully checked and monitored during the welding construction process and after earthquakes to ensure that the strength bearing and deformation capacities meeting the requirements.

Funding This study funded by graduate research and innovation projects of Jiangsu province.

Declarations

Conflict of interest The author(s) declared no potential conflicts of interest with respect to the research, authorship, and/or publication of this article.

References

AISC. (1994). *In Proceedings of the AISC Special Task Committee on the Northridge Earthquake*. American Institute of Steel Construction.

Anderson, J. C., Gourley, B. C., & Green, M. (1995). *Case Studies of Steel Moment Frame Building Performance in the Northridge Earthquake of January 17, 1994*. Federal Emergency Management Agency.

Albedah, A., Bouiadjra, B. B., & Benyahia, F. (2018). Effects of adhesive disband & thermal residual stresses on the fatigue life of cracked 2024–T3 aluminum panels repaired with a composite patch. *International Journal of Adhesion and Adhesives, 87*, 22–30.

An, G., Jeong, S. M., & Park, J. (2018). Ductile crack initiation criterion with mismatched weld joints under dynamic loading conditions. *Journal of Nanoscience and Nanotechnology, 18*(3), 2252–2257. https://doi.org/10.1166/jnn.2018.14959

Belytschko, T., & Black, T. (1999). Elastic crack growth in finite elements with minimal remeshing. *International Journal for Numerical Methods in Engineering, 45*(5), 601–620. https://doi.org/10.1002/(SICI)1097-0207(19990620)45:5%3c601::AID-NME598%3e3.0.CO;2-S

Belytschko, T., Goangseup, Z., & Xu, J. X. (2003). The extended finite element method for arbitrary discontinuities. *Computational Mechanics Theory and Practice, 14*(16), 453–468.

Baptista, R., Santos, T., Marques, J., Guedes, M., & Infante, V. (2018). Fatigue behavior and microstructural characterization of a high strength steel for welded railway rails. *International Journal of Fatigue, 117*, 1–8. https://doi.org/10.1016/j.ijfatigue.2018.07.032

Babazadeh, A., & Khedmati, M. R. (2019). Empirical formulations for estimation of ultimate strength of cracked continuous unstiffened plates used in ship structure under in-plane longitudinal compression. *Engineering Failure Analysis, 100*, 470–484. https://doi.org/10.1016/j.engfailanal.2019.02.051

Chi, W. M., Deierlein, G. G., & Ingraffea, A. R. (2000). Fracture toughness demands in welded beam-column moment connections. *Journal of Structural Engineering, 126*(1), 88–97. https://doi.org/10.1061/(ASCE)0733-9445(2000)126:1(88)

Citarella, R. (2009). Non-linear MSD crack growth by DBEM for a riveted aeronautic reinforcement. *Advances in Engineering Software, 40*(4), 253–259. https://doi.org/10.1016/j.advengsoft.2008.04.007

Engelhardt, M. D., & Sabol, T. A. (1997). Seismic-resistant steel moment connections: developments since the 1994 Northridge earthquake. *Progress in Structural Engineering and Materials, 1*(1), 68–77. https://doi.org/10.1002/pse.2260010112

Gross, J. L. (1998). A connection model for the seismic analysis of welded steel moment frames. *Engineering Structures, 20*(4–6), 390–397. https://doi.org/10.1016/S0141-0296(97)00090-4

Huang, X. W., Tong, L. W., Zhou, F., & Chen, Y. Y. (2013). Prediction of fracture behavior of beam-to-column welded joints using micromechanics damage model. *Journal of Constructional Steel Research, 85*, 60–72. https://doi.org/10.1016/j.jcsr.2013.02.014

Joh, C., & Chen, W. (1999). Fracture strength of welded flange-bolted web connections. *Journal of Structural Engineering, 125*(5), 565–571. https://doi.org/10.1061/(ASCE)0733-9445(1999)125:5(565)

Jones, S. L., Fry, G. T., & Engelhardt, M. D. (2002). Experimental evaluation of cyclically loaded reduced beam section moment connections. *Journal of Structural Engineering, 128*(4), 441–451. https://doi.org/10.1061/(ASCE)0733-9445(2002)128:4(441)

JGJ/T 101–2015. (2015). *Specification for Seismic Test of Buildings*. China Architecture and Building Press.

Kauffmann, E. J., Fisher, J. W. (1996). Fracture analysis of failed moment frame weld joints produced in full-scale laboratory tests and buildings damaged in the Northridge Earthquake. Sacramento: Technical Report SAC-95–08.

Liu, X. Y., Wang, Y. Q., Xiong, J., & Shi, Y. J. (2017). Damage behavior of steel beam-to-column connections under inelastic cyclic loading. *Journal of Zhejiang University-Science A, 18*(11), 910–926. https://doi.org/10.1631/jzus.A1600520

Miller, D. K. (1998). Lessons learned from the Northridge earthquake. *Engineering Structures, 20*(4–6), 249–260.

Matos, C. G., & Dodds, R. H. (2000). Modeling the effects of residual stresses on defects in welds of steel frame connections. *Engineering Structures, 22*(9), 1103–1120. https://doi.org/10.1016/S0141-0296(99)00055-3

Matos, C. G., & Dodds, R. H. (2001). Probabilistic modeling of weld fracture in steel frame connections part I: Quasi-static loading. *Engineering Structures, 23*(8), 1011–1030. https://doi.org/10.1016/S0141-0296(00)00107-3

Matos, C. G. (2002). Probabilistic modeling of weld fracture in steel frame connections part II: Seismic loading. *Engineering Structures, 24*(6), 687–705.

Ma, S. Q., Gu, L. X., Yuan, Y. W., Zhao, W. Z., & Huang, X. F. (2014). Research on influence of welding defects on fatigue life of EMU aluminum-alloy car body. *Journal of the China Railway Society, 36*(2), 42–48. (in Chinese).

Popov, E. P., Yang, T. S., & Chang, S. P. (1998). Design of steel MRF connections before and after 1994 Northridge earthquake. *Engineering Structures, 20*(12), 1030–1038.

Pokrovskii, V. V., Sidyachenko, V. G., & Ezhov, V. N. (2018). Fatigue crack growth in the base metal and weld of the combustion chamber casing of an aircraft gas-turbine engine. *Strength Mater, 50*(4), 636–643.

Qin, T., Xu, X., & Shuailing, L. (2021). A model for ultra low cycle fatigue damage prediction of structural steel. *Journal of Constructional Steel Research*. https://doi.org/10.1016/j.jcsr.2021.106956

Razavi, S. M. J., Ayatollahi, M. R., Sommitsch, C., & Moserc, C. (2017). Retardation of fatigue crack growth in high strength steel S690 using a modified stop-hole technique. *Engineering Fracture Mechanics, 2017*(169), 226–237. https://doi.org/10.1016/j.engfracmech.2016.11.013

SAC Joint Venture. (1995). *Interim Guidelines: Evaluation, Repair, Modification and Design of Welded Steel Moment Frame Structures*. Federal Emergency Management Agency.

SAC Joint Venture. (1995). *Analytical & Field Investigations of Buildings Affected by the Northridge Earthquake of January 17, 1994*. Federal Emergency Management Agency.

SAC Joint Venture. (1995). *Parametric Analytic Investigation of Ground Motion and Structural Response, Northridge Earthquake of January 17, 1994*. Federal Emergency Management Agency.

SAC Joint Venture. (1996). *Experimental Investigations of Beam-Column Subassemblages*. Federal Emergency Management Agency.

Song, J. L., & Ellingwood, B. R. (1999). Seismic reliability of special moment steel frames with welded connections: I. *Journal of Structural Engineering, 125*(4), 357–371.

Syed, A. K., Fitzpatrick, M. E., & Moffatt, J. E. (2014). Evolution of residual stress during fatigue crack growth in an aluminium specimen with a bonded crack retarder. *Composite Structures, 117*, 12–16.

Tremblay, R., Filiatrault, A., & Bruneau, M. (1996). Seismic design of steel buildings: lessons from the 1995 Hyogo-Ken Nanbu earthquake. *Canadian Journal of Civil Engineering, 23*(3), 727–756.

Xu, G., & Ellingwood, B. R. (2011). Probabilistic robustness assessment of pre-Northridge steel moment resisting frames. *Journal of Structural Engineering, 137*, 925–934.

Xie, S. M., Wang, T., & Chen, Y. J. (2017). Stability analysis of EMU aluminum alloy car-body with initial defect. *Journal of Dalian Jiaotong University, 38*(6), 25–29. (in Chinese).

Yan, X., & Huang, X. (2015). Prediction of fatigue life reliability for ship details based on crack growth. *Journal of Shanghai Jiaotong University, 49*(2), 214–219. (in Chinese).

Yang, Y. T., Wang, Y., Yang, F., & An, Q. (2019). Influence of weld details on fracture behavior of connections using high-strength steel. *Journal of Constructional Steel Research, 153*, 578–587. https://doi.org/10.1016/j.jcsr.2018.11.004